Dalton Transactions

Accepted Manuscript

ROYAL SOCIETY OF CHEMISTRY

www.rsc.org/dalton

Switching and redox isomerism in first-row transition metal complexes containing redox active Schiff base ligands

Ashok Sasmal[a], Eugenio Garribba[b], Carlos J. Gómez-García[c], Cédric Desplanches[d], Samiran Mitra[*a]

[a]Department of Chemistry, Jadavpur University, Raja S.C. Mullick Road, Kolkata-700032, West Bengal, India

[b]Department of Chemistry and Pharmacy, and Center for Biotechnology Development and Biodiversity Research, University of Sassari, Via Vienna 2, I-07100 Sassari, Italy

[c]Institutode Ciencia Molecular (ICMol), Universidad de Valencia, ParqueCientífico, 46980 Paterna, Spain

[d]CNRS, Université de Bordeaux, ICMCB, 87 Avenue du Dr. A. Schweitzer, Pessac, F-33608, France

** Corresponding author: Tel: + 91-33-2414 6666 (Extn. 2779); fax: + 91-33-2414 6414*

E-mail address: samiranju92@gmail.com

Abstract

The reversible redox isomerisms in first row transition metals complexes of the type ML2 were studied. The six ML_2 complexes (M = Mn^{III} (**1**), Fe^{II} (**2**), Co^{III} (**3**) , Ni^{II} (**4**), Cu^{II} (**5**) and Zn^{II} (**6**)) were synthesized with a redox active Schiff base ligand [2-(3, 5-di-*tert*-butyl-2-hydroxyphenylamino)-4-chlorophenol](**LH_3**) presenting different oxidation states from -2 to 0 (L^{2-}, L^{-} and L^{0}). EPR spectra and magnetic susceptibility measurements indicate the presence of complexes of the type $[Mn^{III}(L^{2-})(L^{-})]$ (**1**) with S = 1/2, $[Fe^{II}(L^{-})_2]$ (**2**) with S = 2, $[Co^{III}(L^{2-})(L^{-})]$ (**3**) with S = 1/2, $[Ni^{II}(L^{-})_2]$ (**4**) with S = 1, $[Cu^{II}(L^{-})_2]$ (**5**) with S = 1/2 and $[Zn^{II}(L^{-})_2]$ (**6**) with S = 0 at high temperature. Temperature and solvents influence the electronic structures of the species and give several valence tautomers. At low temperatures these complexes present thermally

induced metal-to-ligand (**1-5**) or ligand-to-ligand (in **6**) electron transfer (partial or total), resulting in compounds of the type $[Mn^{IV}(L^{2-})_2]$ (**1'**) with S = 1/2, $[Fe^{III}(L^{-})(L^{2-})]$ (**2'**) with S = 1, $[Co^{III}(L^{-})(L^{2-})]$ (**3'**) with S = 1/2, $[Ni^{III}(L^{2-})(L^{-})]$ (**4'**) with S = 0, $[Cu^{II}(L^{2-})(L^{0})]$ (**5'**) with S = 1/2 and $[Zn^{II}(L^{2-})(L^{0})]$ (**6'**) with S = 1. These electron transfers agree with the general trend in the redox potentials of the first row transition metal ions from Mn(II) to Zn(II) and it is possible to prepare and stabilize reversibly switchable tautomeric forms in transition metal complexes with redox-active ligands.

Introduction

The current interest on developing molecule-based spin electronic devices such as switches, memories, or spin valves has stimulated the study of responsive switchable molecular materials with magnetic and/or conducting properties. Molecules exhibiting inter conversion between energetically close-lying electronic states are actively investigated as possible candidates for information storage[1]. There are several classes of potentially switchable molecules, like thermochromic compounds[2], mixed valence compounds[3,4], spin crossover complexes[5] and valence tautomers[6-9]. The last term defines two molecules related by an intramolecular electron-transfer process, *i.e.* A–D and A^{-}–D^{+}, thus involving two electronic isomers characterized by different charge distributions and then by different physical and chemical properties. Redox active metal complexes are excellent building blocks for switchable materials, due to their ability to switch between two spin states via a reversible reduction-oxidation process in response to an external stimulus. Nonetheless, for most non-innocent redox active complexes, the absence of strong cooperative interactions (energy gap between two states, HOMO-LUMO) makes the reverse intramolecular electron-transfer (IET) process very fast, thus preventing a genuine bistability.

A large number of complexes of the first-row transition metal complex of general formula $M(N\text{-}N)(diox)_2$ / $M(Cat\text{-}N\text{-}SQ)_2$ (M = Mn, Fe, Co, Ni, Cu and Zn; N-N = 2,2'-bipyridine(bpy), *N,N,N′,N′*-tetramethylethylenediamine (tmeda), 1,10-phenanthroline (phen), bis(2-pyridyl)ketone $(py)_2CO$), 5-nitro-1,10-phenanthroline (NO_2phen), dipyrido-[3,2-a:2',3'-c]phenazine(dppz), and 4,5-diazafluoren-9-one (dafl); diox = catecholato, semiquinoato; Cat-N-SQ = 2-hydroxy-3,5-di-*tert*-butyl-1-phenyl)imino)-3,5-di-*tert*butyl-1,2-benzoquinone) along with biquinone Schiff base transition metal complex have been synthesized and explored[6-13]. No interconversion in the solid

state was observed, as evidenced by the lack of changes in the variable magnetic susceptibility data.

We now report design and synthesis of a non-symmetric biquinone Schiff base ligand [2-(3, 5-di-*tert*-butyl-2-hydroxyphenylamino)-4-chlorophenol](**LH_3**) (Scheme **1**) containing the same N_2O_4 donor set as the previously reported symmetric biquinone Schiff base analogues by removing the two *tert*-butyl groups from a phenyl ring. This will reduce the covalency of the interaction between metal and ligand. The fully deprotonated form of this ligand (H_3L) can exist in different oxidation states, in particular 0 (L^0 with S = ½), -1 (L^- with S = 0), -2 ($L^{2-}$with S = ½) and -3 (L^{3-} with S = 0) (Scheme **2**) .

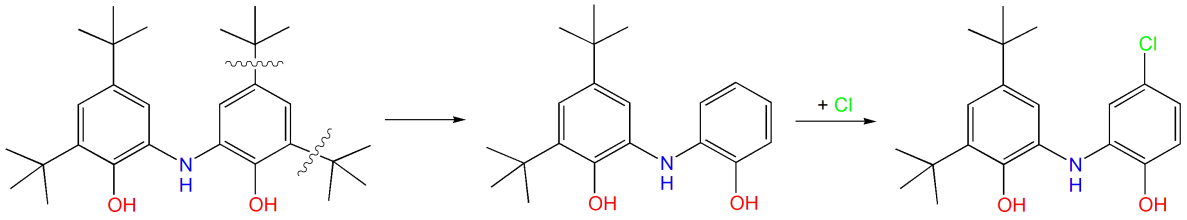

Scheme1: Design of the target ligand

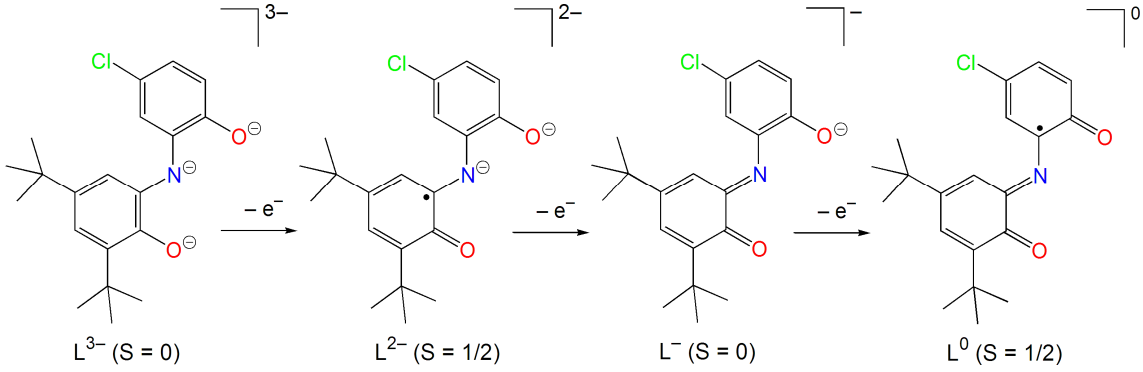

Scheme 2: Oxidation states of the ligand

Experimental Section

Materials. 3,5-di-*tert*butylcatechol, 2-amino-5-chlorophenol were purchased from Sigma Aldrich. The metal salts were purchased from local suppliers. All solvents and reagents were of reagent grade and used as received without further purification.

Synthesis of the Ligand H_3L

To a solution of 3,5-di-*tert*butylcatechol (2.25 g; 10 mmol) and triethylamine (0.2 mL) in *n*-hexane (50 mL), solid 2-amino-5-chlorophenol (1.43 g, 10 mmol) was added. The resulting solution was stirred in air three hours. Then a white (brownish) solid was precipitated and collected by filtration, washed with *n*-hexane, and air-dried. Yield: 0.65 g (70 %). Elemental analysis. Found: C, 69.01; H, 7.50; N, 3.99. Calc. for $C_{20}H_{26}ClNO_2$: C, 69.05; H, 7.53; N, 4.03%. FT-IR (KBr, ν_{max}/cm^{-1}): 3422(b), 2959(s), 2868(w), 2675(w), 1596(b), 1478(b), 1421(w), 1358(w), 1306(w), 1236(s), 1201(w), 1117(w), 1054(b), 1032(w), 990(w), 930(w), 873(w), 854(w), 809(w), 656(w). UV-vis, $\lambda_{max}(CH_3CN)/nm$: 226(ε/dm^3 mol^{-1} cm^{-1} 4390), 286(1600), 300(1460). ^1H NMR (300 MHz, $CDCl_3$, Me_4Si) δ_H: 2.01 (s, 18H, t-Butyl), 1.44 (s, 3H, t-Butyl)ppm. ESI-MS, *m*/*z*: [M] = 348.

Synthesis of Complexes

$[Mn^{III}(L^{2-})(L^{-})]\cdot CH_3CN$ (1)

To a acetonitrile solution of the ligand, H_3L (0.694g, 2 mmol), the methanol solution of (30 mL), manganese(II) nitrate, $Mn(NO_3)_2\cdot 3H_2O$(0.36 g, 2 mmol) was added. Then 0.2 mL of NEt_3 was added and the color of the solution was changed to green. After stirring the solution in presence of air for 2 h, a dark greenish brown microcrystalline product of **1** was collected by filtration. Yield: 0.73 g (70 %). Elemental analysis: Found: C, 64.10; H, 6.25; N, 5.30. Calc. for $C_{42}H_{49}Cl_2MnN_3O_4$: C, 64.20; H, 6.29; N, 5.35 %. FT-IR (KBr, ν_{max}/cm^{-1}): 3422(b), 2958(s), 2868(m), 1527(w), 1446(s), 1413(w), 1383(s), 1363(m), 1310(s), 1233(s), 1180(s), 1125(w), 1108(s), 1077(m), 1024(m), 994(s), 901(m), 845(m), 811(m), 774(w), 750(w), 709(w), 633(m), 586(m), 541(w), 520(w), 493(w). UV-vis, $\lambda_{max}(CH_3CN)/nm$: 232 (ε/dm^3 mol^{-1} cm^{-1} 8730), 294 (4130), 344(4435), 443 (2110), 468(2050), 584(1810), 802(1550), 915(1850). ^1H NMR (300 MHz, $CDCl_3$, Me_4Si) δ_H: 2.00(s, 18H, t-Butyl), 1.59(s, 3H, t-Butyl) ppm. ESI-MS, *m*/*z*: [M^+] =744.

$[Fe^{II}(L^{-})_2]$ (2)

To a acetonitrile solution of the ligand, H_3L (0.694 g, 2 mmol), the methanol solution (30 mL), of anhydrous ferric(III) chloride, $FeCl_3$ (0.312 g, 2 mmol) was added. The 0.2 mL of NEt_3 was added and then the color of the solution was changed to green. After stirring of the solution in presence of air for 2 h, a brown microcrystalline product of **2** was obtained and collected by filtration. Yield: 0.65 g (65 %). Elemental analysis. Found: C, 64.40; H, 6.20; N, 3.72. Calc. for $C_{40}H_{46}Cl_2FeN_2O_4$: C, 64.44; H, 6.22; N, 3.76%. FT-IR (KBr, ν_{max}/cm^{-1}): 2957(s), 2868(w), 1560(w), 1527(m), 1508(w), 1446 (s), 1414(s), 1380(m), 1362(s), 1340(w), 1310(s), 1233(s), 1180(s), 1125(w), 1108(s), 1077(m), 1025(s), 994(s), 925(s), 900(s), 845(m), 810(m), 774(w), 750(w), 709(m), 676(w), 634(w), 586(m), 541(w), 520(w), 492(w). UV-vis, $\lambda_{max}(CH_3CN)/nm$: 232(ε/dm^3 mol^{-1} cm^{-1} 5100), 391(2660), 512(1140), 774(1430). ^1H NMR (300 MHz, $CDCl_3$, Me_4Si) δ_H: 2.02(s, 9H, t-Butyl) ppm. ESI-MS, *m*/*z*: $[M + 2H^+] = 747$.

$[Co^{III}(L^{2-})(L^{-})]$ (3)

To a acetonitrile solution of the ligand, H_3L (0.694 g, 2 mmol), the methanol (30 mL) of anhydrous cobalt(II) nitrate $Co(NO_3)_2$ (0.4 g, 2 mmol) was added. The 0.2 mL of NEt_3 was added and the color of the solution was changed to green. After stirring of the solution in presence of air for 2 h, a black microcrystalline product of **3** was obtained and collected by filtration. Yield: 0.76 g (70 %). Elemental analysis. Found: C, 64.13; H, 6.14; N, 3.70. Calcd. for $C_{40}H_{46}Cl_2CoN_2O_4$: C, 64.17; H, 6.19; N, 3.74%. FT-IR (KBr, ν_{max}/cm^{-1}): 2957(s), 1542(w), 1508(m), 1490(m), 1405(m), 1388(m), 1363(s), 1322(w), 1286(w), 1250(s), 1202(s), 1108(w), 1064(s), 1020(m), 980(s), 930(w), 894(s), 837(w), 807(w), 747(s), 705(s), 636(w), 615(s), 592(w), 535(w), 501(s). UV-vis, $\lambda_{max}(CH_3CN)/nm$): 231(ε/dm^3 mol^{-1} cm^{-1} 10220), 295(4845), 344(5200), 441(2510), 468(2450), 548(2190), 800(1850), 920(2214). ^1H NMR (300 MHz, $CDCl_3$, Me_4Si) δ_H: 6.93 (s, 1H, Ar-H), 2.02(s, 9H, t-Butyl), 1.62(s, 9H, t-Butyl)ppm. ESI-MS, *m*/*z*: $[M^+] = 748$, $[M + Na^+] = 771$.

$[Ni^{II}(L^{-})_2]\cdot CH_3OH$ (4)

To a acetonitrile solution of the ligand, H_3L (0.694 g, 2 mmol), the methanol (30 mL) of nickel nitrate, $Ni(NO_3)_2$ (0.4 g, 2 mmol) was added. The 0.2 mL of NEt_3 was added and the color of the solution was changed to green. After stirring of the solution in air for 2h, a dark green

microcrystalline product of **4** was obtained and collected by filtration. Yield: 0.65 g (60%). Elemental analysis. Found: C, 63.05; H, 6.40; N, 5.55. Calc. for $C_{41}H_{50}Cl_2NiN_2O_5$: C, 63.10; H, 6.46; N, 5.59%. FT-IR (KBr, ν_{max}/cm^{-1}): 3477(b), 2958(s), 2868(w), 1591(w), 1534(w), 1502(s), 1407(s), 1388(w), 1363(s), 1344(s), 1291(s), 1250(s), 1205(m), 1165(w), 1130(s), 1101(s), 1063(s), 1022(s), 977(s), 919(s), 893(s), 848(m), 822(m), 796(s), 739(w), 689(w), 658(m), 627(m), 607(m), 527(m), 495(m). UV-vis, $\lambda_{max}(CH_3CN)/nm$: 239(ε/dm^3 mol^{-1} cm^{-1} 1980), 420(1080), 764(2030), 823(1790). ^1H NMR (300 MHz, $CDCl_3$, Me_4Si) δ_H: 2.00(s, 9H, t-Butyl), 1.59(s, 9H, t-Butyl) ppm. ESI-MS, *m*/*z*: $[M + 3H^+]$= 751, $[M+3H^+ + Na^+]$ = 775.

$[Cu^{II}(L^-)_2]$ (5)

To a acetonitrile solution of the ligand, H_3L (0.694 g, 2 mmol), the methanol (30 mL) of copper nitrate, $Cu(NO_3)_2$ (0.4 g, 2 mmol) was added. The 0.2 mL of NEt_3 was added and the color of the solution was changed to green. After stirring of the solution for 2 h, a brown microcrystalline product of **5** was obtained and collected by filtration. Yield: 0.60 g (54 %). Elemental analysis. Found: C, 63.70; H, 6.06; N, 3.65. Calcd. for $C_{40}H_{46}Cl_2CuN_2O_4$: C, 63.78; H, 6.16; N, 3.72%. FT-IR (KBr, ν_{max}/cm^{-1}): 3448(b), 3089(s), 2959(s), 2869(w), 1508(w), 1481(s), 1459(w), 1384(s), 1363(w), 1276(s), 1198(s), 1150(m), 1114(m),1084(s), 1024(w), 967(m), 911(w), 878(w), 838(w), 798(m), 746(w), 636(w), 596(m), 503(w). UV-vis, $\lambda_{max}(CH_3CN)/nm$: 366 (ε/dm^3 mol^{-1} cm^{-1} 2070). ^1H NMR (300 MHz, $CDCl_3$, Me_4Si) δ_H: 2.03(s, 9H, t-Butyl), 1.62(s, 9H, t-Butyl) ppm. ESI-MS, *m*/*z*: $[M^+]$ = 752.

$[Zn^{II}(L^-)_2]$ (6)

To a acetonitrile solution of the ligand, H_3L (0.694 g, 2 mmol), the methanol (30 mL) of zinc nitrate, $Zn(NO_3)_2$ (0.4 g, 2 mmol) was added. The 0.2 mL of NEt_3 was added and the color of the solution was changed to green. After stirring of the solution for 2 h, a dark green microcrystalline product of **6** was obtained and collected by filtration. Yield: 0.75 g (68 %). Found : C, 63.58; H, 6.09; N, 3.68. Calcd. for $C_{40}H_{46}Cl_2ZnN_2O_4$: C, 63.62; H, 6.14; N, 3.71%. FT-IR (KBr, ν_{max}/cm^{-1}): 3448(b), 2959(s), 2870(w), 1507(w), 1431(w), 1408(s),1384(s), 1363(s), 1345(s), 1319(w),1292(s), 1252(s), 1205(m), 1166(w), 1130(s), 1098(w), 1082(w), 1064(s), 1022(s), 976(s), 919(s), 892(s), 850(w), 823(w), 794(s), 740(s), 684(w), 658(s), 604(s), 526(s), 495(s). UV-vis, $\lambda_{max}(CH_3CN)/nm$: 238(ε/dm^3 mol^{-1} cm^{-1} 1780), 393(540), 426(487), 723(1780). ^1H

NMR (300 MHz, $CDCl_3$, Me_4Si) δ_H: 2.01(s, 9H, t-Butyl), 1.61(s, 9H, t-Butyl) ppm. ESI-MS, *m*/*z*: $[M^+] = 755$, $[M+Na^+] = 777$.

Physical measurements

The Fourier Transform Infrared spectra (4000-400 cm^{-1}) of ligand and complexes were recorded on a Perkin-Elmer RX-I FT-IR spectrophotometer in solid KBr matrix. The electronic spectra of the ligand and the complex were recorded at room temperature on an Agilent 8453 Diode array spectrophotometer in acetonitrile medium. Elemental analyses (C, H, and N) were carried out with a Perkin-Elmer 2400 II elemental analyzer. The ^1H NMR spectrum of the ligand was recorded on a Bruker 300 MHz FT-NMR spectrometer using trimethylsilane as internal standard in $CDCl_3$ and DMSO-d_6. The positive ion ESI-MS for the ligand L and complexes were performed in a QTOF micro mass spectrometer. EPR spectra were recorded from 0 to 10000 Gauss in the temperature range 77-298 K with an X-band (9.4 GHz) Bruker EMX spectrometer equipped with a HP 53150A microwave frequency counter. EPR parameters reported in the text were obtained by simulating the spectra with the computer program Bruker WinEPR SimFonia. Variable-temperature magnetic susceptibility measurements were carried out on polycrystalline samples with a Quantum Design MPMS-5S SQUID magnetometer under an applied magnetic field of 5000 Oe in the temperature range 2-300 K. Diamagnetic corrections were estimated from Pascal's tables, and magnetic data were corrected for diamagnetic contributions of the sample holder.

X-Ray crystallography

Good quality single crystals of complexes **1-4** were mounted on a Bruker APEX-II CCD diffractometer equipped with graphite monochromated Mo Kα radiation (λ = 0.71073 Å) fine-focus sealed tube. The intensity data were collected using ω scan at 293 and for 3-LT, it was 150K. Data refinement and reduction were performed using the Bruker SAINT[14a] software. Multi-scan absorption corrections were applied empirically to the intensity values (T_{min} = 0.924 and T_{max} = 0.943 for **1**, T_{min} = 0.882 and T_{max} = 0.897 for **2** and T_{min}=0.904 and T_{max}=0.927 for **3-RT,** T_{min}=0.902 and T_{max}=0.926 for **3-LT,** T_{min}=0.909 and T_{max}=0.932 for **4**) using SADABS[14a]. The structures were solved by direct methods using the program SHELXS-2013[14b] and refined with full-matrix least-squares based on F^2 using program SHELXL-2014[14b]. All non-hydrogen

atoms were refined anisotropically. C-bound hydrogen atoms were placed geometrically and refined using a riding model approximation. There were disordered acetonitrile molecule in 1 and methanol molecule in 4 which were removed using the SQUEEZE routine from PLATON software[14c]. The squeeze outputs are appended in the CIF file. The molecular graphics were prepared using ORTEP[14d] and Mercury programs. Crystallographic data and structure refinement parameters for the complexes are summarized in Table **1**. The crystal structures of complexes **5** and **6** could not be solved since we could not obtain good single crystals.

Table 1: Crystallographic data and structural refinement for complexes **1-4**

compound	**1**	**2**	**3-RT**	**3-LT**	**4**
Empirical formula	$C_{40}H_{46}Cl_2MnN_2O_4$	$C_{40}H_{46}Cl_2FeN_2O_4$	$C_{40}H_{46}Cl_2CoN_2O_4$	$C_{40}H_{46}Cl_2CoN_2O_4$	$C_{40}H_{46}Cl_2N_2NiO_4$
Formula weight	744.63	745.54	748.62	748.62	748.38
Crystal system	Triclinic	Monoclinic	Monoclinic	Monoclinic	Triclinic
Space group	*P-1*	*P21/n*	*P21/n*	*P21/n*	*P-1*
Temperature (K)	293	293	293	150	293
a /Å	11.8538(5)	11.8964(6)	11.7645(3)	11.705(5)	12.151(5)
b /Å	12.8470(6)	20.6638(11)	20.6993(6)	20.458(5)	13.045(5)
c /Å	14.7605(7)	15.8441(7)	15.8548(4)	15.778(5)	14.498(5)
α /°	68.292(2)	90	90	90	66.617(5)
β /°	80.533(2)	98.025(3)	97.786(2)	97.938(5)	79.473(5)
γ/°	81.195(2)	90	90	90	79.908(5)
V /Å^3	2049.50(16)	3856.7(3)	3825.32(18)	3742(2)	2060.4(14)
Z	2	4	4	4	2
d_{calc} (g cm^{-3})	1.207	1.284	1.300	1.329	1.206
μ(mm^{-1})	0.491	0.571	0.630	0.644	0.639
F(000)	782	1568	1572	1572	788
θ range (deg)	1.7, 27.5	1.6, 27.6	1.6, 27.2	1.6, 27.5	1.7, 27.5
Measured reflections	31190	33937	61536	50775	32043
Independent reflections	9351	8806	8487	8498	9261
R(int)	0.032	0.024	0.083	0.107	0.042
Observed reflections [*I*>2σ(*I*)]	6932	3146	4804	5285	5926
Goodness-of-fit on F^2	0.98	0.85	0.89	0.90	0.89
Final *R* indices [*I* >2σ(*I*)]	R_1 = 0.0529	R_1 = 0.0689	R_1 = 0.0509	R_1 = 0.0507	R_1 = 0.0456
	wR^2= 0.1647	wR^2 = 0.1972	wR^2 = 0.1676	wR^2 = 0.1519	wR^2=0.1303
Δ_{min} and Δ_{max} (e.Å^{-3})	-0.54, 0.75	-0.46, 0.26	-0.27, 0.26	-0.55, 0.28	-0.41, 0.41

Description of the crystal structures

$[Mn^{III}(L^{2-})(L^{-})]\cdot CH_3CN$ (1), $[Fe^{II}(L^{-})_2]$ (2), $[Co^{III}(L^{2-})(L^{-})]$ (3) and $[Ni^{II}(L^{-})_2]\cdot CH_3OH$ (4).

Single crystal X-ray analysis reveals that complexes **1-4** are very similar. Complexes **1** and **4** crystallize in the triclinic space group P-1 whereas complexes **2** and **3** crystallize in the monoclinic space group $P2_1/n$. The asymmetric units of these complexes contain one metal atom and two ligands, forming discrete ML_2 complexes in all cases. Additionally, in **1** and **4** there are also acetonitrile and methanol molecules respectively. The four complexes are formed with a metal:ligand ratio of 1:2 (Fig. **1**) and contain two tridentate ligands coordinated to the metal atom in a meridional fashion with an O, N, O-donor set. The geometry around the metal atom is six-coordinate with a N_2O_4 environment, in which the phenolato oxygens occupy the *cis*-positions and the central N atoms are disposed in trans with N-M-N bond angles close to 180º (Table **2**). Complex **1** is a *cis* isomer with respect to the *tert*-butyl groups whereas the other three complexes present a *trans* disposition of the *tert*-butyl groups. The coordination sphere MN_2O_4 is a distorted octahedron with M-O and M-N bond distances typical in these kinds of octahedral complexes (Table **2, 3**). The six-membered rings of the iminobenzo-semiquinonate parts display the typical quinoid distortions in all the complexes. The C-O and C-N bond lengths in complexes **2**-**4** are short, approaching towards double bonds The torsion angles between the imine bond and the chlorobenzene rings are 4.3(5)º and 10.8(5)º in **1**, 9.7(8)º and 7.7(5)º in **2**, 8.2(6)º and 9.4(6)º in **3-RT,** 8.1(6)º and 9.1(6)º in **3-LT**, 2.4(5)º and 10.8(5)º in **4** for the two ligands. At 150K, the C-C bond lengths increase indicating a higher reduction degree of the ligands in **3-LT**. The Cl···Cl interactions (3.385 and 3.321 Å) lead to the formation of a supramolecular dimers in **1** and **4**. The C-Cl bonds lengths of the two ligands are in the range 1.728-1.743 Å, indicating significant charge delocalization into these C-Cl bonds[4]. Views of the packing of the discrete ML_2 complexes **1-4** is shown in the supporting information.

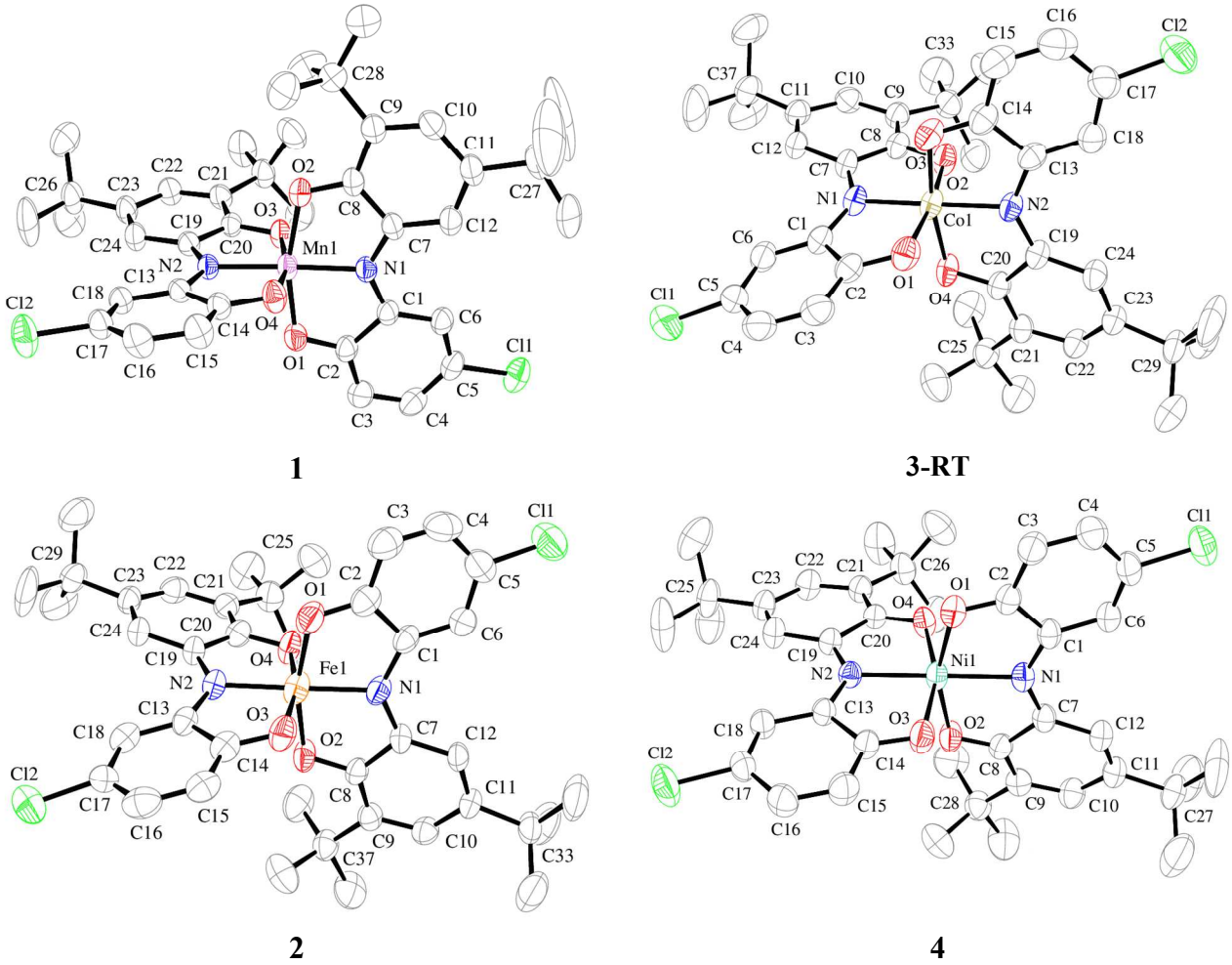

Fig. 1. Structure of complexes **1-4** showing the labeling scheme.

Table 2: Selected bond distances (Å) in complexes **1**-**4**

1		2		3RT		3LT		4	
Mn1-O1	1.908(2)	Fe1-O1	1.900(3)	Co1-O1	1.888(2)	Co1-O1	1.904(2)	Ni1-O1	2.038(2)
Mn1-O2	1.919(2)	Fe1-O2	1.900(3)	Co1-O2	1.879(2)	Co1-O2	1.908(2)	Ni1-O2	2.089(2)
Mn1-O3	1.897(19)	Fe1-O3	1.897(3)	Co1-O3	1.907(2)	Co1-O3	1.890(2)	Ni1-O3	2.022(2)
Mn1-O4	1.885(2)	Fe1-O4	1.891(3)	Co1-O4	1.914(2)	Co1-O4	1.882(2)	Ni1-O4	2.036(2)
Mn1-N1	1.903(2)	Fe1-N1	1.897(4)	Co1-N1	1.861(2)	Co1-N1	1.862(2)	Ni1-N1	2.016(2)
Mn1-N2	1.917(2)	Fe1-N2	1.907(4)	Co1-N2	1.867(2)	Co1-N2	1.862(2)	Ni1-N2	2.029(2)
O1-C2	1.316(3)	O1-C2	1.316(6)	O1-C2	1.322(4)	O1-C1	1.297(4)	O1-C1	1.269(3)
O2-C8	1.309(3)	O2-C8	1.314(5)	O2-C8	1.322(4)	O2-C8	1.282(3)	O2-C8	1.256(3)
O3-C20	1.311(3)	O3-C14	1.313(6)	O3-C14	1.292(4)	O3-C14	1.318(4)	O3-C14	1.269(3)
O4-C14	1.316(3)	O4-C20	1.311(6)	O4-C20	1.278(4)	O4-C20	1.314(3)	O4-C20	1.255(3)
N1-C1	1.380(3)	N1-C1	1.382(6)	N1-C1	1.365(4)	N1-C1	1.359(4)	N1-C1	1.353(3)
N1-C7	1.361(3)	N1-C7	1.376(6)	N1-C7	1.357(4)	N1-C7	1.344(4)	N1-C7	1.329(3)
N2-C13	1.383(3)	N2-C13	1.386(6)	N2-C13	1.361(4)	N2-C13	1.371(4)	N2-C13	1.360(3)
N2-C19	1.373(3)	N2-C19	1.358(6)	N2-C19	1.338(4)	N2-C19	1.361(4)	N2-C19	1.340(4)

Table 3: Selected bond angles (º) in complexes **1**-**4**

1		2		3RT		3LT		4	
O1-Mn1-O2	164.59(9)	O1-Fe1-O2	164.97(14)	O1-Co1-O2	171.68(10)	O1-Co1-O2	170.34(9)	O1-Ni1-O2	160.20(8)
O1-Mn1-O3	92.89(8)	O1-Fe1-O3	91.87(15)	O1-Co1-O3	91.67(10)	O1-Co1-O3	91.58(10)	O1-Ni1-O3	91.43(8)
O1-Mn1-O4	92.12(9)	O1-Fe1-O4	91.13(15)	O1-Co1-O4	90.49(10)	O1-Co1-O4	90.45(10)	O1-Ni1-O4	94.57(8)
O1-Mn1-N1	82.99(9)	O1-Fe1-N1	82.80(15)	O1-Co1-N1	86.18(10)	O1-Co1-N1	85.73(10)	O1-Ni1-N1	81.19(8)
O1-Mn1-N2	94.90(9)	O1-Fe1-N2	98.04(15)	O1-Co1-N2	96.25(10)	O1-Co1-N2	95.20(10)	O1-Ni1-N2	100.95(8)
O2-Mn1-O3	88.16(8)	O2-Fe1-O3	91.31(14)	O2-Co1-O3	90.24(10)	O2-Co1-O3	90.61(9)	O2-Ni1-O3	92.73(8)
O2-Mn1-O4	90.74(9)	O2-Fe1-O4	89.47(14)	O2-Co1-O4	89.03(10)	O2-Co1-O4	88.69(9)	O2-Ni1-O4	87.45(8)
O2-Mn1-N1	81.66(9)	O2-Fe1-N1	82.18(14)	O2-Co1-N1	85.58(11)	O2-Co1-N1	84.69(10)	O2-Ni1-N1	79.03(8)
O2-Mn1-N2	100.47(9)	O2-Fe1-N2	96.91(14)	O2-Co1-N2	91.97(11)	O2-Co1-N2	94.33(10)	O2-Ni1-N2	98.80(8)
O3-Mn1-O4	165.08(8)	O3-Fe1-O4	165.42(15)	O3-Co1-O4	169.94(10)	O3-Co1-O4	171.90(9)	O3-Ni1-O4	161.74(8)
O3-Mn1-N1	98.55(9)	O3-Fe1-N1	99.88(15)	O3-Co1-N1	95.34(10)	O3-Co1-N1	96.02(10)	O3-Ni1-N1	99.85(9)
O3-Mn1-N2	82.01(9)	O3-Fe1-N2	83.24(15)	O3-Co1-N2	85.70(10)	O3-Co1-N2	86.22(10)	O3-Ni1-N2	82.04(8)
O4-Mn1-N1	96.01(9)	O4-Fe1-N1	94.66(15)	O4-Co1-N1	94.61(10)	O4-Co1-N1	91.95(10)	O4-Ni1-N1	98.11(8)
O4-Mn1-N2	83.57(9)	O4-Fe1-N2	82.21(15)	O4-Co1-N2	84.30(10)	O4-Co1-N2	85.79(10)	O4-Ni1-N2	79.89(8)
N1-Mn1-N2	177.83(9)	N1-Fe1-N2	176.76(15)	N1-Co1-N2	177.34(11)	N1-Co1-N2	177.56(11)	N1-Ni1-N2	177.16(9)

Magnetic studies of the complexes 1-6

$[Mn^{III}(L^{2-})(L^{-})]$ (1'): The thermal variation of the product of the molar magnetic susceptibility per Mn(III) ion times the temperature ($\chi_m T$) for **1** shows a room temperature value of ca. 0.50 $cm^3.K.mol^{-1}$ (Fig. **2**). This behavior indicates that complex **1** contains one unpaired electron, as a result of the strong antiferromagnetic coupling of the central low-spin (LS) S = 1 Mn(III) ion (d^4) with one S = 1/2 L^{2-} ligand. EPR spectrum of **1** at room temperature is consistent with a spin state of S = ½ (see below). When the temperature is decreased, $\chi_m T$ shows a smooth decrease to reach a value of ca. 0.38 $cm^3.K.mol^{-1}$ at 2 K. This smooth and linear decrease indicates that **1** is essentially a paramagnet with a temperature independent paramagnetic (tip) contribution of ca. 260 x 10^{-6} $cm^3.mol^{-1}$. At very low temperatures **1** show a progressive decrease that could be due to the presence of weak intermolecular antiferromagnetic interactions. This behavior indicates that in **1** there is a metal to ligand electron transfer operating at any temperature to give $[Mn^{IV}(L^{2-})_2]$.

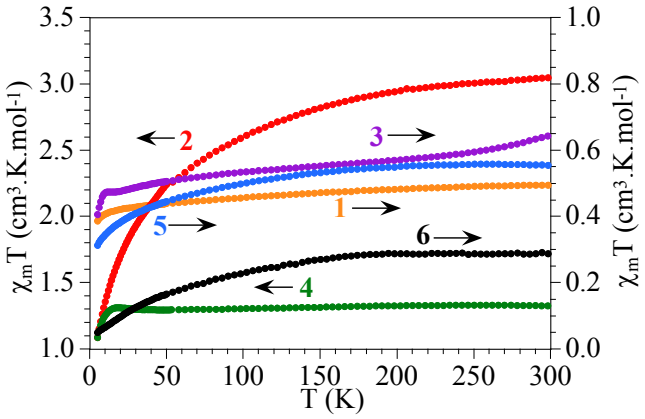

Fig. 2. Thermal variation of the $\chi_m T$ product per metal ion for complexes **1-6**.

$[Fe^{II}(L^{-})_2]/[Fe^{III}(L^{-})(L^{2-})]$ (2/2'): The thermal variation of the $\chi_m T$ product per iron ion for compound **2** shows a room temperature value of ca. 3.05 $cm^3.K.mol^{-1}$ (Fig. 2), which is the expected value for a high-spin (HS), d^6 Fe(II) with S = 2. When the temperature is lowered, $\chi_m T$ shows a progressive decrease to reach a value of ca. 1.1 $cm^3.K.mol^{-1}$ at 2 K, close to the expected one for an S = 1 spin ground state, in agreement with EPR measurements (see below). This behavior suggests the presence of a strong antiferromagnetic Fe-Fe coupling or a metal to ligand

electron transfer, resulting in $[Fe^{III}(L^{2-})(L^{-})]$ containing a LS Fe(III) ion (S = ½) ferromagnetically coupled with a L^{2-} ligand also with a S = ½ ground spin state, resulting in a S = 1 spin state. Since there is no short Fe-Fe pathway to justify a strong antiferromagnetic coupling, the electron transfer seems to be the more plausible explanation. This electron transfer leads to a $[Fe^{III}(L^{2-})(L^{-})]$ complex containing a S = ½ Fe(III) ion ferromagnetically coupled with an S =1/2 L^{2-} ligand, leading to a S = 1 ground spin state at very low temperatures, in agreement with the EPR measurements (see below).

$[Co^{III}(L^{-})(L^{2-})]$ (3'): The thermal variation of $\chi_m T$ per cobalt ion for compound **3** shows a room temperature value of ca. 0.60 $cm^3.K.mol^{-1}$ that smoothly decreases to reach a value of ca. 0.5 $cm^3.K.mol^{-1}$ at low temperatures (Fig. 2). This behavior indicates that in this case we must have a metal to ligand electron transfer already at room temperature, leading to a complex of the type $[Co^{III}(L^{-})(L^{2-})]$ (**3'**) with a S = 0 LS Co(III) ion (d^6) plus a S = ½ L^{2-} ligand. The extra contribution observed can be attributed to the small temperature independent paramagnetic (tip) contribution expected for Co(III) ions.

$[Ni^{II}(L^{-})_2]/[Ni^{III}(L^{-})(L^{2-})]$ (4/4'): The thermal variation of $\chi_m T$ per Nickel ion for compound **4** shows a room temperature value of ca. 1.20 $cm^3.K.mol^{-1}$, which is the expected one for an isolated Ni(II) monomer with $g \approx 2.2$. When the temperature is decreased, $\chi_m T$ remains constant down to ca. 5 K. Below this temperature $\chi_m T$ shows an abrupt decrease to reach a value of ca. 1.05 $cm^3.K.mol^{-1}$ (Fig. **2**). This behavior indicates that this compound presents isolated paramagnetic Ni(II) monomers with a zero field splitting at very low temperatures. The observed $\chi_m T$ value in complex **4** confirms the proposed formula $[Ni^{II}(L^{-})_2]$ with two unpaired electrons (S = 1) located on the Ni(II) ion and with two S = 0, L^{-} ligands. The presence of a small fraction of $[Ni^{III}(L^{2-})(L^{-})]$ (**4'**) at low temperatures with a strong antiferromagnetic interaction between the unpaired electron on the Ni(III) ion and the unpaired electron on the L^{2-} ligand, might also be at the origin of the sharp decrease observed at very low temperatures. EPR spectroscopy confirms the presence of a small amount of $[Ni^{III}(L^{2-})(L^{-})]$ in the solid state (see below).

$[Cu^{II}(L^{-})_2]/[Cu^{II}(L^{0})(L^{2-})]$ (5/5'): The thermal variation of $\chi_m T$ per Cu(II) ion for compound **5** shows a room temperature value of ca. 0.55 $cm^3.K.mol^{-1}$, above the expected value for an isolated Cu(II) monomer with $g = 2$. This behavior agrees with the presence of $[Cu^{II}(L^{-})_2]$ units with one unpaired electron located on the Cu(II) ion (S = 1/2) plus a small amount of

$[Cu^{II}(L^0)(L^{2-})]$ resulting from an inter-ligand electron transfer (as observed in complex 6, see below). When the temperature is lowered, $\chi_m T$ shows a progressive decrease to reach a value of ca. 0.30 $cm^3.K.mol^{-1}$ at 2 K (Fig. **2**). This behavior suggests that the small fraction of complex $[Cu^{II}(L^0)(L^{2-})]$ shows an antiferromagnetic coupling resulting in a S = ½ spin ground state.

$[Zn^{II}(L^-)_2]$/$[Zn^{II}(L^0)(L^{2-})]$ (6/6'): The magnetic properties of this compound show a very low $\chi_m T$ value at any temperature (once corrected the TIP contribution, Fig. **2**), indicating that the major component in **6** must be a diamagnetic green complex of the type $[Zn(L^-)_2]$. Nevertheless, complex **6** can also be present as its isomeric red and paramagnetic form $[Zn(L^{2-})(L^0)]$ (**6'**) containing two unpaired electrons, one on each ligand where the oxidation states of the two coordinated ligands in the complex differ formally by *two* electrons. The low value of the magnetic susceptibility suggests the presence of a small, although not negligible, fraction of $[Zn^{II}(L^{2-})(L^0)]$ with two interacting unpaired electrons per molecule.[8b]

EPR studies

The EPR spectra of the polycrystalline powders were recorded at room temperature and 77 K. The spectra of complex **1**, reported in Fig. **3,** show significant differences as a function of the temperature. At 298 K, the spectrum of **1** is characterized by an isotropic signal with a single absorption centered at g = 2.038 and a line width (expressed by the value of ΔH_{pp}) of 105 G (Fig. 3a, blue line). At 77 K, three EPR signals are observed with different line widths, centred at three g values (Fig. 3a, red line). The better resolution at 77 K might be due to the narrowing of the signals with decreasing temperature. These observations are in agreement with the rhombic EPR spectrum of **1** detected in solution (Fig. 3b) that can be simulated with the following values of g and A: g_x = 1.983, g_y = 2.036, g_z = 2.020, and $A_x = 143.5\times10^{-4}$ cm^{-1}, $A_y = 80.6\times10^{-4}$ cm^{-1}, $A_z = 4.0\times10^{-4}$ cm^{-1}. Values so large for the hyperfine coupling constants indicate that the spin density is concentrated on the metal rather than on the ligand, i.e. the hyperfine structure arises from the coupling of the unpaired electron with the ^{55}Mn (I = 5/2) nucleus. This spectrum is similar to those of other species with an electron localized on Mn atoms[7]. Overall EPR spectra can be interpreted on the basis of a spin state S = ½, as suggested by the variation of the molar magnetic susceptibility with the temperature.

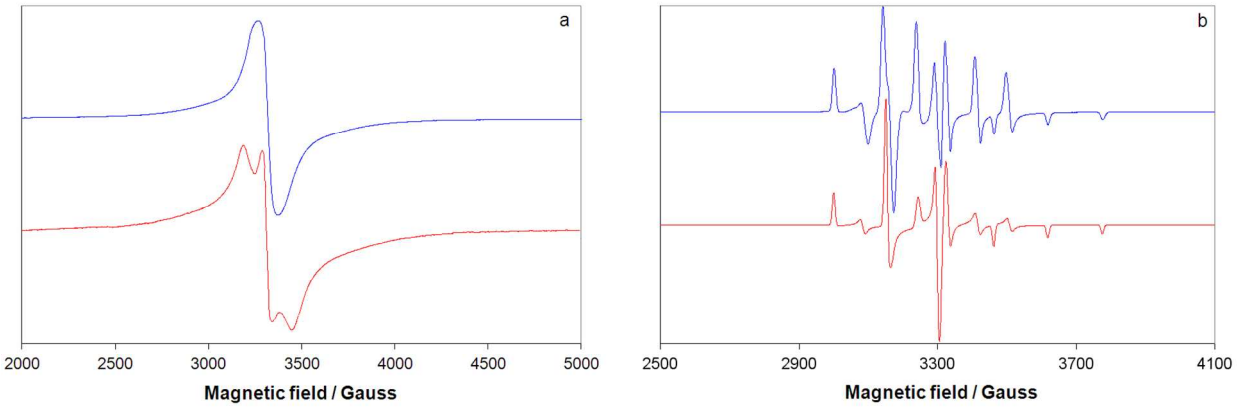

Fig. 3. (a) X-band EPR spectra of the polycrystalline complex **1** at 298 K (blue) and 77 K (red). (b) Experimental (blue) and simulated (red) X-band EPR spectrum of **1** dissolved in a mixture of CH_2Cl_2/toluene (60:40 v/v).

The EPR spectra of a polycrystalline sample of **2** recorded at 298 and 77 K are characterized by a narrow signal at g ≈2 and a very weak signal at g ≈ 4.3 that can be observed at low temperatures (See ESI Fig. **S2a**). Since the high spin S = 2 $[Fe^{II}(L^{-})_2]$ complex is expected to be EPR silent, the spectrum observed for **2** has to be attributed to the presence of a small fraction of the complex $[Fe^{III}(L^{-})(L^{2-})]$ resulting from an electron transfer from the Fe(II) to one of the L^{-} ligands, in agreement with the susceptibility measurements (see above). The central narrow line at g ≈ 2 arises from the coupling of S = ½ species (the LS Fe(III) ion and the L^{2-} ligand). A deeper look at this central line shows that two absorptions attributable to a S = 1 state are detected (See ESI Fig. **S2b**). The weak line centered at g ≈ 4.3 corresponds to the half field ΔM_s = ± 2 forbidden transition indicative of the presence of a ferromagnetic coupling between both S = ½ systems, also in agreement with the susceptibility measurements (see above). When **2** is dissolved in CH_2Cl_2/toluene 60:40 v/v, the intensity of the EPR signal is very weak and only the resonance centred at g ~ 2.0 can be detected. This indicates that in solution $[Fe^{II}(L^{1-})_2]$ species is predominant and that only a very small amount of $[Fe^{III}(L^{1-})(L^{2-})]$ exists (see ESI Fig. **S3**).

At 298 K complex **3** shows an EPR spectrum with a single isotropic line at g = 1.997 that splits into two absorptions at 77 K, one of them assignable to a radical species with g = 1.996 and a very small ΔH_{pp} of 13.1 G (Fig. 4a).[11] It must be noticed the difference in the central signals detected for **1** and **3** at 77 K (Fig. 3a and 4a): they are centered, respectively, at g=2.045 and 1.996 and are characterized by ΔH_{pp} of 59 and 13 G, indicating that for **1** the unpaired electron

resides on the metal, whereas in **3** it is located on the ligand. This result are compatible with a complex of the type $[Co^{III}(L^{2-})(L^{-})]$ (**3'**) with a S = ½ L^{2-} ligand, in agreement with the susceptibility measurements. As observed in the iron derivative **2**, the complex $[Co^{III}(L^{2-})(L^{-})]$ results from an electron transfer from the Co(II) to the ligand. Fig. 4b shows the EPR spectrum of complex **3** recorded in a mixture of CH_2Cl_2/toluene (60:40 v/v) (blue) together with its simulation (in red). The resonances are due to the coupling of an unpaired electron with ^{59}Co (I = 7/2) nucleus; no resolved superhyperfine coupling to the ^{14}N nuclei has been observed. It was simulated with $g_x = 2.005$, $g_y = 1.992$, $g_z = 1.987$, and $A_x = 7.6\times10^{-4}$ cm^{-1}, $A_y = 24.0\times10^{-4}$ cm^{-1}, $A_z = 3.6\times10^{-4}$ cm^{-1}. The small values of the ^{59}Co hyperfine coupling constants suggest that the spin density is delocalized over the ligand. The data are consistent with a complex of the type $[Co^{III}(L^{-})(L^{2-})]$, also found for similar ligands.[11] This assignment rules out the species $[Co^{II}(L^{-})_2]$ for which higher value of ^{59}Co *A* is expected[15].

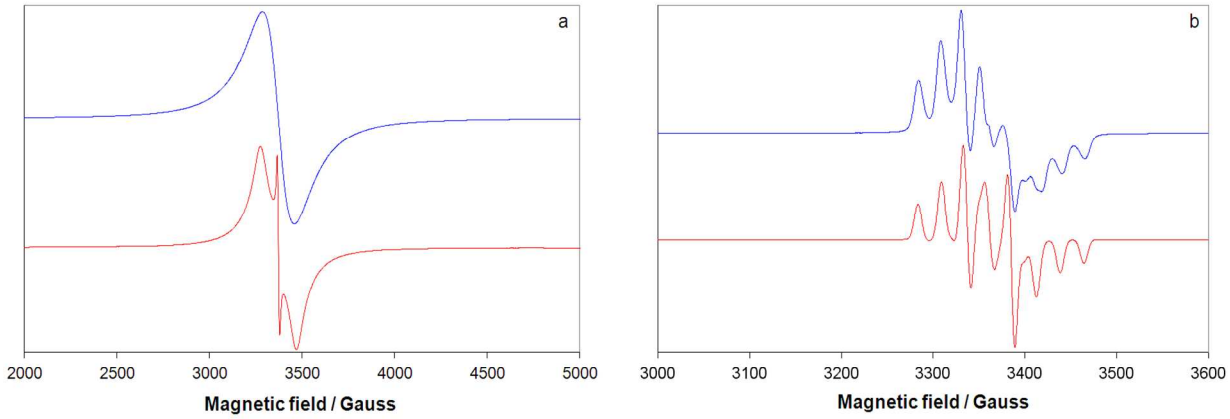

Fig. 4. (a) X-band EPR spectra of the polycrystalline complex **3** at 298 K (blue) and 77 K (red). (b) Experimental (blue) and simulated (red) X-band EPR spectrum of **3** dissolved in a mixture of CH_2Cl_2/toluene (60:40 v/v).

The EPR spectra of **4** as a polycrystalline powder and in CH_2Cl_2/toluene (60:40 v/v) are represented in ESI Fig. **S4**. The intensity in all the cases is very weak, suggesting a complex of the type $[Ni^{II}(L^{-})_2]$, with the metal atom EPR-silent due to the zero field splitting (ZFS) of the S = 1 spin ground state, and the ligands L^{-} in a S = 0 spin ground state. The weak signal, detected at 298 K and 77 K, has to be attributed to a small amount of $[Ni^{III}(L^{-})(L^{2-})]$ (**4'**). In fact, the narrow absorption at g = 2.004 is attributable to a radical (L^{2-} with S = ½, indicated by an asterisk in ESI Fig. **S4a**) and the signals at $g_{\perp}$ = 2.295 and $g_{\|}$ ~ 2.000 to Ni^{III} ion (d^7

configuration) with a d_{z^2} ground state (indicated by two arrows in Fig. **S4a**).[16] The formation of $[Ni^{III}(L^{-})(L^{2-})]$, supported also by susceptibility measurements, is due to the transfer of an electron from Ni(II) to the ligand. In a mixture of CH_2Cl_2/toluene (60:40 v/v), $[Ni^{II}(L^{-})_2]$ is the predominant species and only a small amount of $[Ni^{III}(L^{-})(L^{2-})]$ can be observed (Fig. **S4b**).

The EPR spectra of a polycrystalline sample of **5** (Fig. **5a**) does not vary significantly as a function of the temperature. No transitions attributable to radical species are observed. The *g* values are in the order: $g_z >> g_y \sim g_x > g_e$ and are indicative of a $d_{x^2-y^2}$ ground state.[17] The parameters at 298 K are $g_z = 2.201$ and $A_z = 208.2\times10^{-4}$ cm^{-1}. These data are in agreement with a complex of the type $[Cu^{II}(L^{-})_2]$, where the only paramagnetic species is the Cu(II) ion (d^9, S = 1/2). In a mixture of CH_2Cl_2/toluene (60:40 v/v) (Fig. **5b**), the EPR signal due to the Cu(II) ion does not change ($g_z = 2.203$ and $A_z = 208.4\times10^{-4}$ cm^{-1}) although a new narrow signal at g ≈ 2 can be clearly observed. This spectrum is compatible with the presence of $[Cu^{II}(L^{-})_2]$ as the main species, and of either a $[Cu^{III}(L^{-})(L^{2-})]$ (arising from a metal to ligand electron transfer; d^8 Cu^{III} ion with S = 0, L^{2-} ligand with S = ½, L^{-} ligand with S = 0) or a $[Cu^{II}(L^{0})(L^{2-})]$ (arising from a inter-ligand electron transfer; d^9 Cu^{II} ion with S = ½, L^{2-} ligand with S = ½, L^{0-} ligand with S = 1/2) as the minor species; this is in agreement with the susceptibility measurements (see above).

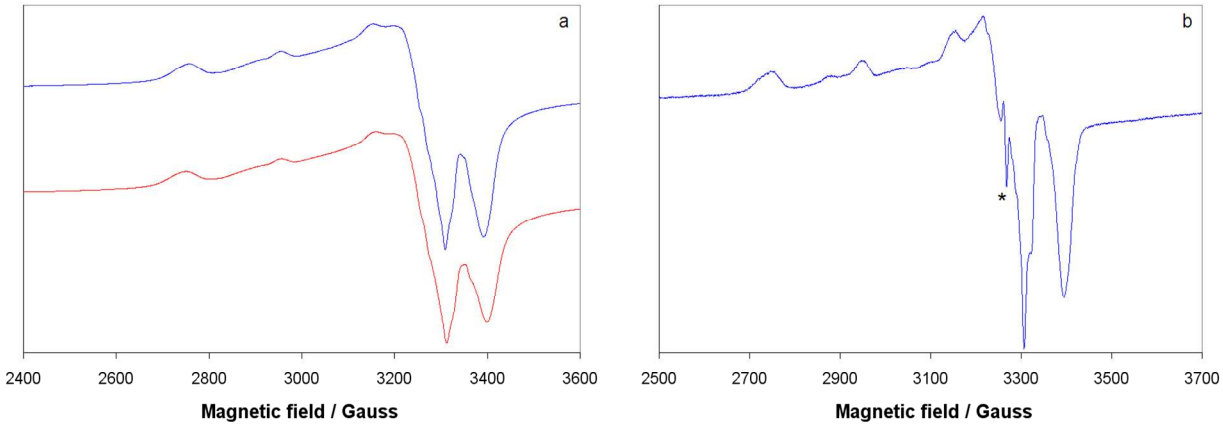

Fig. 5. (a) X-band EPR spectra of the polycrystalline complex **5** at 298 K (blue) and 77 K (red). (b) X-band EPR spectrum of **5** dissolved in a mixture of CH_2Cl_2/toluene (60:40 v/v). An asterisk indicates the signal of the L^{2-} form of the ligand ($S = 1/2$).

With Zn(II), two possible structures can exist: $[Zn^{II}(L^{-})_2]$ (**6**) and $[Zn^{II}(L^{0})(L^{2-})]$ (**6'**). Compounds like $[Zn^{II}(L^{-})_2]$ are diamagnetic and no EPR signal should be observed.[9] In contrast, $[Zn^{II}(L^{0})(L^{2-})]$ is paramagnetic (if the coupling of the two S =1/2 ligands is ferromagnetic) and

EPR response is expected.[8b] The EPR spectra recorded on a polycrystalline sample of **6** are shown in Fig. **6a**. The spectra are similar at 298 K and 77 K: they show a narrow band at g = 2.004 and a signal of a triplet state, due to the coupling of the L^{2-} and L^{0} forms of the ligand with S = 1/2; the separation of the parallel component is twice the separation of the perpendicular region, as expected from the background theory. The formulation $[Zn^{II}(L^{0})(L^{2-})]$ accounts for the experimental spectra, which are comparable with those of other systems with two unpaired electron localized on organic radicals.[18] In contrast what was observed for Fe, Co, Ni, species and analogously to what happens with Cu, in this case an intra-ligand electron transfer from one to another L^{-} ligand takes place. Fig. **6b** displays the X-band EPR spectrum of **6** at 77 K in a mixture CH_2Cl_2/toluene (60:40 v/v). This spectrum resembles that of the paramagnetic species formed by *N*,*N*-(bis(2-hydroxy-di-3,5-*tert*-butylphenyl)amine and is consistent with the formulation $[Zn^{II}(L^{0})(L^{2-})]$.[8b]

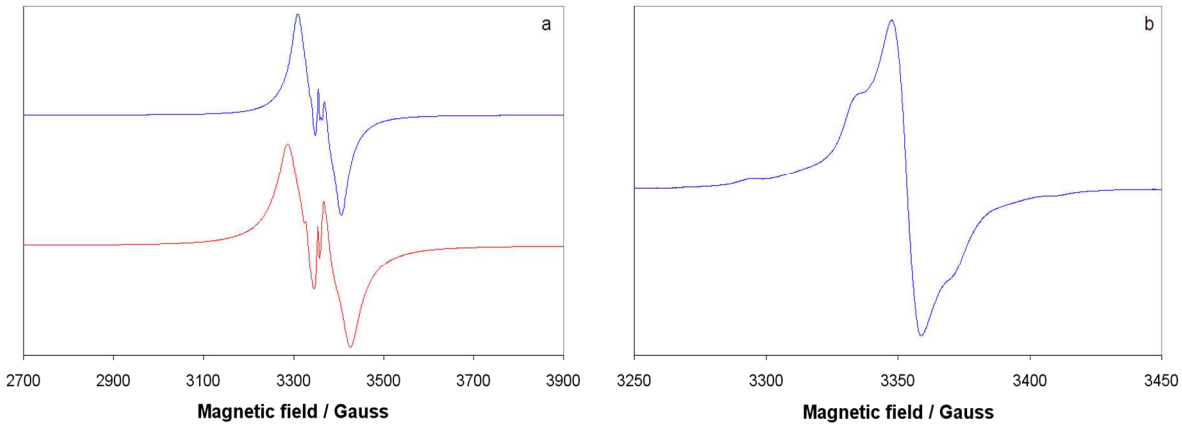

Fig. 6. (a) X-band EPR spectra of the polycrystalline complex **6** at 298 K (blue) and 77 K (red). (**b)** X-band EPR spectrum of **6** dissolved in a mixture CH_2Cl_2/toluene (60:40 v/v).

NMR spectra of the complexes

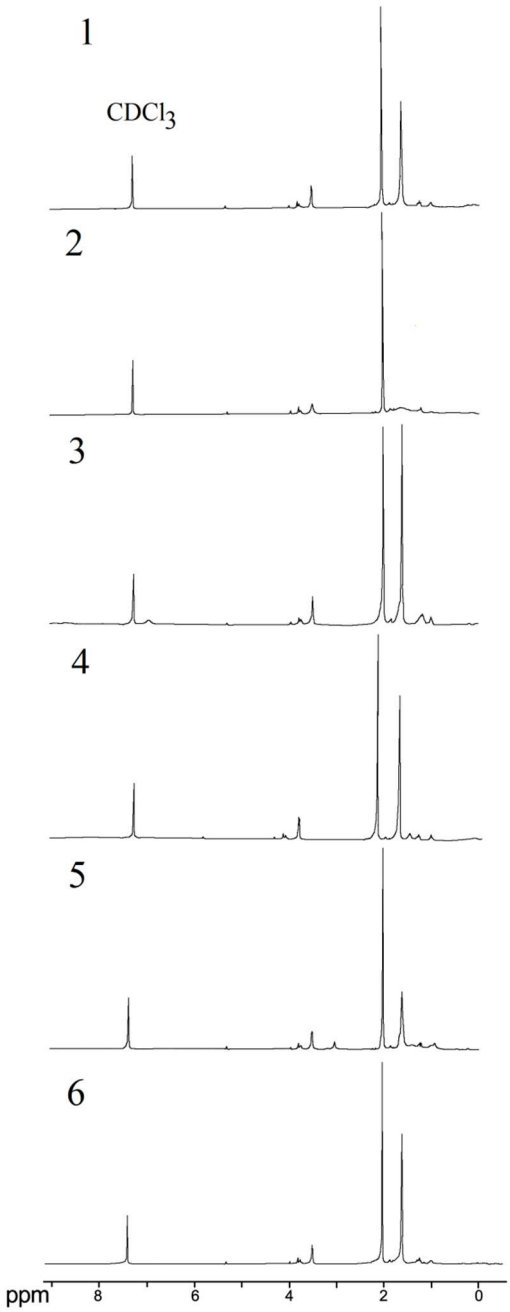

Fig. 7: NMR spectra of the $M(L)_2$ complexes M = Mn (**1**), Fe (**2**), Co (**3**), Ni (**4**), Cu (**5**) and Zn (**6**) recorded at room temperature in $CDCl_3$.

The neutral complexes ML_2, (M = Mn, Fe, Co, Ni, Cu, Zn) exhibit sharp NMR resonances at room temperature. Spectra on ML_2 were recorded in $CDCl_3$ solution at room temperature and

shown in Fig. **7**. Due to the presence of paramagnetic complexes, some of the ring proton resonances broaden and disappear except the *tert*-butyl groups. The proton resonances are observed in the range 3-4 ppm due to solvent molecules present in the complexes. The *tert*-butyl resonances may be assigned to the *tert*-butyl groups associated with carbons of a phenyl ring that become equivalent with the increased rate of rearrangement. The two *meridonal* ligands in a complex are interconverted by twist mechanism. This must result from rapid isomerism on the NMR time scale. Complex **1** shows two sharp singlets in the *tert*-butyl region at 2.0 and 1.59 ppm due to presence of two isoenergic species in quasi – equilibrium. Complex **2** shows one sharp singlet in the *tert*-butyl region at 2.0 ppm may be due to the presence of predominantly one species. Complexes **3** shows two sharp singlets with equal intensities in the *tert*-butyl region at 2.0 and 1.61 ppm due to presence of two isoenergic species in equilibrium. The Ni(II) complex shows two sharp singlets in the *tert*-butyl region at 2.0 and 1.59 ppm. The complex **5** shows two sharp singlets in the *tert*-butyl region at 2.01 and 1.61 ppm. The weak resonance peak of Cu(II) at 1.61ppm suggests one major isomer. The complex **6** shows two sharp singlets in the *tert*-butyl region at 2.01 and 1.60 ppm. This indicates presence of two isomers: $[Zn^{II}(L^{2-})(L^{0})]$ and $[Zn^{II}(L^{-})_2]$.

Conclusion

We have prepared and characterized an extended series of complexes of formula ML_2 where M is a first row transition metal from Mn to Zn and L is a redox-active Schiff base ligand that can exhibit diverse oxidation degrees from -3 to 0. These systems are worth of consideration for two reasons. First, they describe a redox tautomerism involving a manganese and cobalt complex in which the electronic ground states of the two species are well defined. The second and more important reason is the observation of a reversible thermally induced redox isomerism in the solid state and in solution for the iron, nickel, copper and zinc complexes. The EPR spectra and magnetic properties of compounds **1**-**6** show the presence of major complexes that can be formulated as $[Mn^{III}(L^{2-})(L^{-})]$ (**1**) with S = 1, $[Fe^{III}(L^{-})(L^{2-})]$ (**2'**) with S = 1, $[Co^{III}(L^{-})(L^{2-})]$ (**3'**) with S = 1/2, $[Ni^{II}(L^{-})_2]$ (**4**) with S = 1, $[Cu^{II}(L^{-})_2]$ (**5**) with S = 1/2 and $[Zn^{II}(L^{-})_2]$ (**6**) with S = 0 together with minor components formulated as $[Mn^{IV}(L^{2-})_2]$ (**1'**) with S = 1/2, $[Fe^{II}(L^{-})_2]$ (**2**) with S = 2, $[Ni^{III}(L^{2-})(L^{-})]$ (**4'**) with a S = 1 ground state arising from two S = ½ ferromagnetically coupled systems, $[Cu^{II}(L^{2-})(L^{0})]$ (**5'**) with S = 1/2 and $[Zn^{II}(L^{2-})(L^{0})]$ (**6'**) with S = 1, resulting from an intra-molecular metal to ligand (in **1**-**5**) and ligand-to-ligand in **6**. These electron

transfers agree with the general trend in the redox potentials of the first row transition metal ions that show Mn(II), Fe(II), Co(II) and Ni(II) are more easily oxidized than Cu(II) and Zn(II). The synthesis, characterization, and study of these complexes as stable species allow us to establish a new switching molecular array that interconverts reversibly by redox isomerism.

Supporting Information

CCDC no 921246 (**1**), 921247 (**2**), 921248 (**3-LT**), 921249 (**4**) and 984617 (**3-HT**) contain the supplementary crystallographic data for **1, 2, 3-LT**, **4** and **3-HT,** respectively. Tables of bond lengths and bond angles, Figures of complexes, UV-vis spectra, NMR spectra, Mass spectra, PXRD and crystallographic data in CIF format are included in ESI.

Acknowledgements

A. Sasmal acknowledges Council of Scientific and Industrial Research (CSIR), New Delhi, Govt. of India, for awarding Junior and Senior Research Fellowship (JRF & SRF) to him [CSIR Sanction No. 09/096/0586/2009-EMR-I]. We also thank the Spanish MINECO (CTQ-2011-26507) and the Generalitat Valenciana (Prometeo and ISIC-Nano programs) for financial support. Dr. Mitra acknowledges University Grants Commission (UGC), New Delhi, India for awarding Emeritus Fellowship [F.6-6/EMERITUS-2013-14-GEN-2214/(SA-II)] to carry out this work. We also thank Department of chemistry, Jadavpur University for single crystal XRD and PXRD facilities.

References

1. O. Kahn, J. P. Launay, *Chemtronics*, 1988, **3**, 140.
2. W. Linert, Y. Fukuda, A. Camard *Coord. Chem. Rev.* 2001*,* **218***,* 113 –152.
3. J. A. Thomas, *Coord.Chem.Rev* , 2013, **257**, 1555-1563.
4. C. G. Pierpont, *Inorg. Chem.* 2011, **50**, 9766–9772.
5. (a) M. A. Halcrow, *Chem. Commun.,* 2013, **49**, 10890-10892; (b) M. G. Cowan, S. Brooker, *Coord. Chem. Rev.* 2012, **256**, 2944–2971.
6. (a) D. M. Adam, A. Dei, A. L. Rheingold, D. N. Hendrickson, *J. Am. Chem. Soc*, 1993, **115***,* 8221-8229; (b) R. M. Buchanan, C. G. Pierpont, *J. Am. Chem.* Soc. 1980*,* **102**, 4951-4957; (c) C. G. Pierpont, O. -S. Jung, *Inorg. Chem.* 1995, 34, 4281-4283; (d) O. -S. Jung, C. G. Pierpont, *Inorg.Chem.* 1994, **33**, 2227-2235.
7. S. K. Larsen, C. G. Pierpont, *J. Am. Chem. Soc.* 1988, 110*,* 1827-1832.
8. (a) D. Ruiz-Molina, J. Veciana, K. Wurst, D. N. Hendrickson, C. Rovira, *Inorg. Chem.* 2000, **39***,* 617-619; (b) P. Chaudhuri, M. Hess, K. Hildenbrand, E. Bill, T. Weyhermüller, K. Wieghardt, *Inorg. Chem.* **1999**, *38,* 2781-2790; (c) A. Caneschi, A. Cornia, A. Dei, *Inorg. Chem.* 1998, **37***,* 3419-3421.
9. A. Y. Girgis, A. L. Balch, *Inorg. Chem.*, 1975*,* **14***,* 2724-2727.
10. (a) M. J. Cohn, C. –L. Xie, J. -P. M. Tuchagues, C. G. Pierpont, D. N. Hendrickson, *Inorg. Chem.* 1992, **31***,* 5028-5033; (b) A. S. Attia, O. –S. Jung, C. G. Pierpont, *Inorg. Chim. Acta*, 1994, **226**, 91-98; (c) A. S. Attia, S. Bhattacharya, C. G. Pierpont, *Inorg. Chem.* 1995*,* **34***,* 4427-4433.
11. C. L. Simpson, S. R. Boone, C. G. Pierpont, *Inorg. Chem.* 1989, **28**, 4379-4385.
12. G. Speier, J. Csihony, A. M. Whalen, C. G. Pierpont, *Inorg. Chem.* 1996, **35***,* 3519-3524.
13. E. P. Ivakhnenko, A. G. Starikov, V. I. Minkin, K. A. Lyssenko, M. Y. Antipin, V. I. Simakov, M. S. Korobov, G. S. Borodkin, P. A. Knyazev, *Inorg. Chem.*, 2011, **50**, 7022-7032.
14. (a) Bruker (2000, 2008). SADABS, SMART and SAINT. BrukerAXS Inc., Madison, isconsin, USA; (b) G. M. Sheldrick, *ActaCryst*. 2008**, A64**, 112-122; (c) A. L. Spek, Acta Cryst. 2009, **D65**, 148-155; (d) L. J. Farrugia, *J. Appl. Cryst* , 2012, **45**, 849-854.

15. B. de Bruin, E. Bill, E. Bothe, T. Weyhermüller, K. Wieghardt, *Inorg. Chem.*, 2000, **39**, 2936-2947.

16. (a) O. Rotthaus, V. Labet, C. Philouze, O. Jarjayes, F. Thomas, *Eur. J. Inorg. Chem.*, 2008, 4215-4224; (b) J. R. Hartman, M. Y. Combariza, R. W. Vachet, *Inorg. Chim. Acta*, 2004, **357**, 51-58.

17. (a) B. J. Hathaway, D. E. Billing, *Coord. Chem. Rev.*, 1970, **5**, 143-207; (b) E. Garribba, G. Micera, *J. Chem. Ed.*, 2006, **83**, 1229-1232.

18. Y. C. Chen, G. X. Liu, P. F. Wang, H. Xu, X. M. Ren, Y. Song, Y. X. Sui, *Polyhedron* 2007, **26**, 1781-1786.

Table of contents

Switching and redox isomerism in first-row transition metal complexes containing redox active Schiff base ligands

Ashok Sasmal[a], Eugenio Garribba[b], Carlos J. Gómez-García[c], Cédric Desplanches[d], Samiran Mitra*[a]

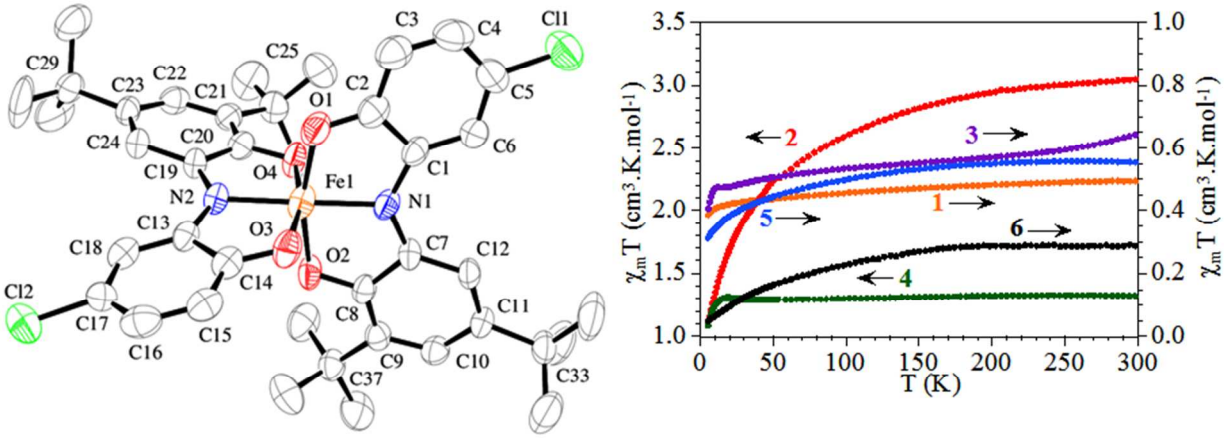

Switching and redox isomerism in first row transition metals complexes through the metal-to-ligand or ligand-to-ligand electron transfer stabilize redox isomeric forms in transition metal complexes with redox-active ligands.